Journal of Power Sources 463 (2020) 228180

Contents lists available at ScienceDirect

Journal of Power Sources

journal homepage: www.elsevier.com/locate/jpowsour

Correlation of electrochemical and mechanical responses: Differential analysis of rechargeable lithium metal cells

Sangwook Kim [a,b], Abhi Raj [a,c], Bin Li [a,**], Eric J. Dufek [a,*], Charles C. Dickerson [a], Hsiao-Ying Huang [b], Boryann Liaw [a], Gorakh M. Pawar [d]

[a] Energy Storage & Advanced Transportation Department, Idaho National Laboratory, Idaho Falls, ID, 83415, USA
[b] Department of Mechanical Engineering, North Carolina State University, Raleigh, NC, 27606, USA
[c] Department of Electrical Engineering, Princeton University, Princeton, NJ, 08542, USA
[d] Materials Science & Engineering Department, Idaho National Laboratory, Idaho Falls, ID, 83415, USA

HIGHLIGHTS

- Tracking mechanical and electrochemical responses of lithium metal batteries.
- Analysis informs on mechanical evolution not discernible by capacity fade.
- dP dV^{-1} analysis provides the opportunity to track mechanical evolution *in operando*.

ARTICLE INFO

Keywords:
Lithium metal battery
Pressure
Mechanical response
Differential analysis

ABSTRACT

Recently, interest in high energy rechargeable lithium metal batteries has increased. Application of pressure has been identified as a distinct means to increase cycle life for these cells, but there is still a disconnect between the evolution of electrochemical and mechanical responses. For this study, lithium/NMC622 pouch cells are cycled under two different pressure conditions and pressure evolution is monitored. Applying pressure with an appropriate experimental setup not only improves performance, but also enables collection of additional information that compliments cell electrochemistry. By jointly comparing differential pressure (dP dV^{-1}) and differential capacity (dQ dV^{-1}) analysis, the combined electrochemical and mechanical cell responses are analyzed. It is found that while little change in cell capacity and dQ dV^{-1} are observed, changes in cell pressure can be used to provide *in operando* information on the lithium metal electrode for full pouch cells. The changes in pressure suggest it is possible to track the evolution of electrode structure from a flatter electrode early in life to a more porous negative electrode prior to the point where cell capacity begins to dramatically fade.

1. Introduction

Conventional lithium-ion batteries (LIBs) which have spurred significant societal impact over the past 30 years have traditionally used graphite as a negative electrode and assorted lithiated metal oxides or lithiated metal phosphates as a positive electrode material. While these chemistries have been successfully adopted for various applications, there is a growing desire to increase the specific energy of cells. One of the most distinct approaches to improve upon the energy density of conventional LIBs is renewed investigation of lithium metal as a negative electrode. When lithium metal is coupled with a high-Ni $LiNi_xMn_yCo_zO_2$ (NMC) positive electrode, there is a possibility to achieve specific energy that may approach 500 Wh kg^{-1} [1]. Lithium is enticing due to a low redox potential (−3.04 V vs S.H.E.), high theoretical capacity (3860 mAh g^{-1}), and a gravimetric density of 0.534 g cm^{-3} [2]. When combined with the improved energy density of high Ni-NMC, which can exceed 200 mAh g^{-1}, there exists a distinct possibility to further reduce the cost of high energy batteries that are crucial for continued adoption of electric vehicles [3,4].

For rechargeable lithium metal batteries (LMBs), one of the challenges with the negative electrode is that a dendritic and mossy lithium surface can form during cycling [5]. These structures, in addition to the

* Corresponding author.
** Corresponding author.
E-mail address: eric.dufek@inl.gov (E.J. Dufek).

https://doi.org/10.1016/j.jpowsour.2020.228180
Received 22 January 2020; Received in revised form 23 March 2020; Accepted 10 April 2020

volume expansion of lithium metal that occurs during charging, result in cracking and formation of new solid-electrolyte interphase (SEI) on the surface of the negative electrode. When both occur, the side reactions between the lithium metal and the electrolyte lead to loss of lithium inventory and the addition of a non-electrochemically active layer. This process consumes both lithium and electrolyte, ultimately perpetuating the formation of increasingly complex surface morphologies [6,7]. As the processes which consume electrolyte and lithium metal advance, significant additional inhibition of lithium deposition and stripping from the negative electrode contribute to slow cell kinetics and divergent rate capability [8]. That is, issues associated with the consumption of the lithium metal negative electrode and electrolyte are the primary factors responsible for capacity fade and the diminished cycle life of LMBs. Simultaneously, higher mechanical stresses generated during charging/discharging processes at the positive electrode can promote structural de-cohesion and cracking of NMC secondary particles [9–11].

While pouch cells are commonly used for many applications due to manufacturing efficiency and stack-ability, swelling is sometimes observed [12]. The expansion is typically linked with the expansion of the active materials in a conventional graphite/metal oxide cell. During cycling, lithium intercalation/de-intercalation results in volume expansion of 7–9% in the positive electrode and ~13% in the negative electrode [13,14]. Gas generation due to electrolyte decomposition leads to additional swelling. Jung et al. [15] reported that gas generation rate of O_2, CO_2, and CO is elevated in layered NMC compared to other electrodes. This is especially true, as the content of Ni in the NMC increases from $LiNi_{0.6}Mn_{0.2}Co_{0.2}O_2$ (NMC622) to $LiNi_{0.8}Mn_{0.1}Co_{0.1}O_2$ (NMC811). The expansion possible in NMC-based LMBs is distinctly greater than LIBs due to the same volume expansion on the positive electrode, but negative electrode expansion is dictated by the capacity charged/discharged during a given cycle. Complicating expansion is the fact that lithium metal deposition is often non-uniform with the formation of dendrites and pits on the lithium metal electrode. Both dendrites and pits can accelerate the formation of inactive (dead) metallic lithium, and may cause near infinite volume expansion [16,17].

Recent works [12,18–20] have reported operando pressure measurement to investigate battery degradation as an effective way to understand the relationship between cell performance and mechanics. Zhang et al. [12] used galvanostatic electrochemical impedance spectroscopy to investigate the effect of external pressure on the performance in graphite/$LiMn_2O_4$ pouch cells. Impedance spectrum changes with increased pressure indicated that external pressure changes the lithium charge transport mechanism at the electrode-electrolyte interface and lithium diffusion in both electrodes. The change in transport is caused by the fact that ionic diffusion is indirectly affected by external pressure as a result of the phase stability of the electrodes [21]. The work from Louli et al. [19] exhibited both a reversible pressure evolution as the cells cycled due to expansion and contraction of silicon-composite negative electrodes during charging and discharging, as well as an irreversible pressure growth concomitant with cycling and mechanical degradation of the composite electrode. Moreover, they showed that irreversible pressure growth is inversely correlated to cell performance based on capacity retention and polarization growth measurements. Louli et al. also correlated pressure changes with SEI growth and loss of lithium inventory. Compared with LIB negative electrode materials, lithium metal electrodes are more reactive with electrolytes, which results in the continual generation of SEI and enhanced isolation of lithium. As cells cycle, the change in lithium thickness is linked with the capacity cycled which, for high energy cells, leads to greater evolution in pressure for LMBs. While it is known that elevated pressures serve to enhance the cycle life of LMBs [22], there have been few studies looking to directly link changes in the mechanical and electrochemical response of LMBs during active cycling.

This paper focuses on linking the evolution of electrochemical and mechanical responses of cells by analyzing pressure and cycling changes measured in lithium/NMC pouch cells. It has been suggested and shown that higher pressure on pouch cells enhances performance by suppressing lithium dendrite development, minimizing isolated particles, and forcing gas from the active surface of the electrode (Fig. 1) [22]. Rather than focusing on applying pressure to enhance performance, this work is focused on using pressure to more directly track and perform real time analysis of different mechanical failure mechanisms which occur during cycling. Differential capacity ($dQ\ dV^{-1}$) curves have been used to characterize and understand distinct changes, which occur in active materials of batteries due to an electrochemical driving force. As such they have been used to investigate aging or degradation mechanisms [23–27]. However, one of the limitations of $dQ\ dV^{-1}$ analysis as a degradation detection method is that the method does not provide insight into mechanical phenomena such as volume expansion of electrodes and cell swelling. In this paper, differential pressure analysis ($dP\ dV^{-1}$) in conjunction with $dQ\ dV^{-1}$ are proposed to correlate and align mechanical and electrochemical phenomena to obtain a more complete picture of cell performance evolution.

2. Experimental procedures

2.1. Cell preparation

Single layer pouch cells (43 mm × 56 mm) were assembled using a single sided $Li[Ni_{0.6}Mn_{0.2}Co_{0.2}]O_2$ (NMC622) positive electrode (9.78 mg cm^{-2} of coating loading, 37.1% porosity, and 38 μm coating thickness) and lithium metal (30 μm of thickness, China Energy Lithium Co.) as the negative electrode. NMC622 laminates were obtained from the Cell analysis, Modeling, and Prototyping (CAMP) facility at Argonne National Laboratory. Each cell used a sheet of Celgard 2325 separator and 300 μL (i.e., 7.5 g Ah^{-1} of positive electrode material) of 1.2 M $LiPF_6$ in a 3:7 wt% blend of ethylene carbonate (EC) and ethyl methyl carbonate (EMC) with 2% vinylene carbonate (VC).

2.2. Cycling test

All cells were cycled at 30 ± 1 °C inside a temperature-controlled environmental chamber (BTZ-133, ESPEC corp.) using a MACCOR Model 2200 (Maccor, Inc.). For the formation cycles, cells were charged to 4.4 V at C/20 (2.5 mA) with a 60 min rest and then discharged to 2.8 V at C/20. After formation cycles, a reference performance test (RPT) was conducted. RPTs were performed in order to assess the changes in the kinetic and thermodynamic aging of the cells. Each RPT included a single C/10 (5 mA) and a single C/20 charging and discharging cycle. Between each RPT half cycle, a rest of 4 h was used to allow the cell to relax to a quasi-equilibrium state. For cycle life aging, 25 cycles (C/10 charging and C/3 discharging, 16.7 mA) with a 15 min rest between half-cycles were used. Upon the completion of each cycle life set, the RPT was repeated prior to continuing cycle life aging.

2.3. Operando pressure measurement

Fig. 2 shows the experimental setup to measure pressure evolution during cycling. The design uses a total of three G10 glass epoxy plates (Ridout Plastics Co. Inc.). The pouch cell was positioned between the first two plates, and 3 LCKD load cells (Omega Engineering Inc.) were placed between the middle and the last plates. In this study, two different initial pressure conditions (e.g., 6.9 (i.e., 1psi) and 69 kPa (i.e., 10psi)) were imposed by adjusting the gap between the plates. These pressures were used based on the minimum pressure which could be applied and still maintain measurement sensitivity (6.9 kPa) and based on previous reports which indicate improved performance for LMBs (69 kPa) [28]. This gap was fixed during cycling and the pressure evolution due to volume changes in the cell were determined using the load cells.

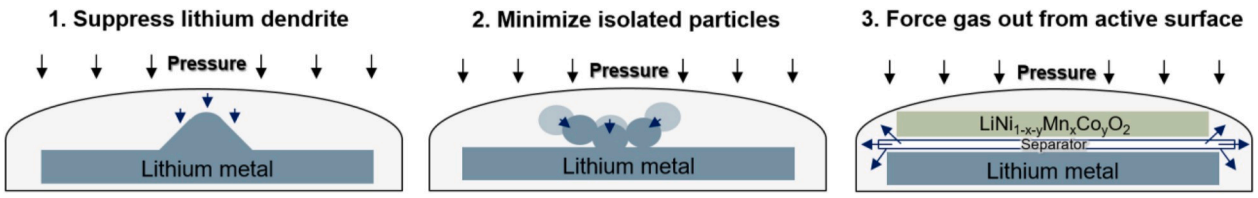

Fig. 1. Three proposed mechanisms in which pressure has been proposed to lead to enhanced performance for LMBs. 1) suppress lithium dendrite [28], 2) minimize isolated particles [28], and 3) force gas out from the active surface area [22].

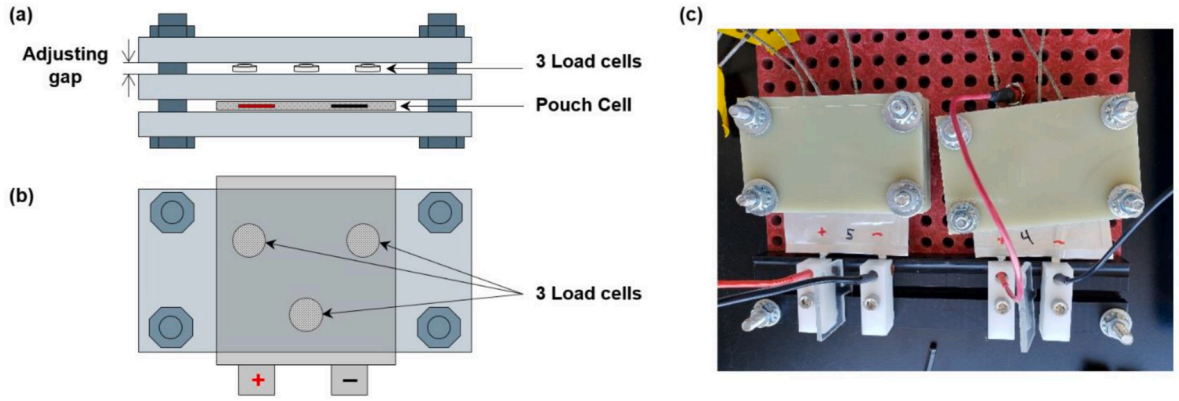

Fig. 2. (a) Side view and (b) top view of a schematic illustration of an experimental setup. (c) Picture of the experimental setup. Additional views of the set-up can be found in Ref. [29].

2.4. Cell characterization

The morphologies of lithium metal electrodes harvested at different stages of cycling were investigated by focused ion beam-scanning electron microscopy (FIB/SEM, Quanta 3D FEG Dual Beam, FEI). The pouch cells were disassembled in an Ar-filled glove box. To remove any residual electrolyte salt, lithium metal electrodes were rinsed with EMC and subsequently dried in the antechamber under vacuum at room

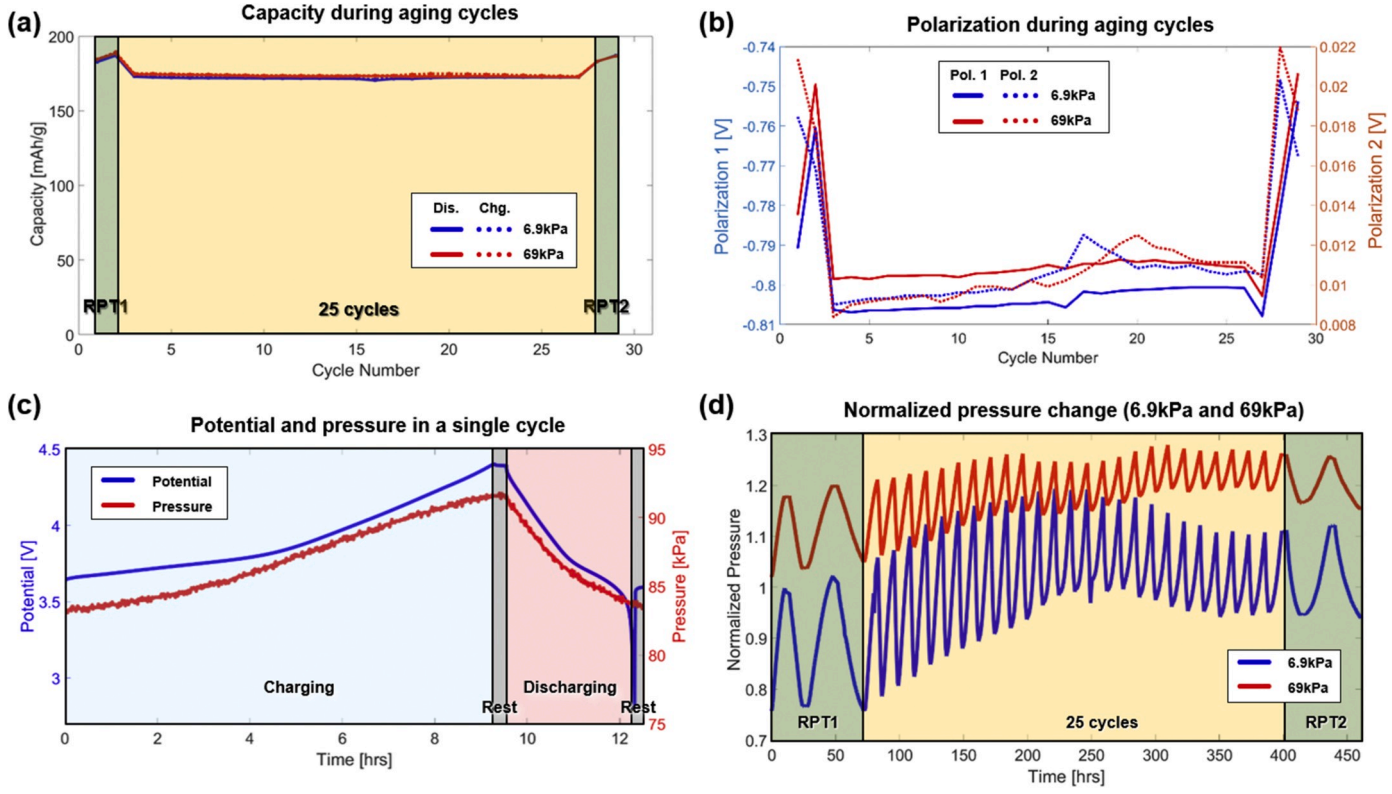

Fig. 3. Cell performances including (a) capacity, (b) polarizations, (c) potential and pressure changes in a single cycle, and (d) normalized pressure changes during the first RPT, aging cycles, and the second RPT.

temperature for 12 h. To avoid exposure to air, the samples were sealed inside an air-tight container and quickly transferred into the FIB-SEM [10,30–32].

3. Results

Shown in Fig. 3a is the capacity during the 25 aging cycles and two RPTs. The capacity fade at both 6.9 kPa and 69 kPa is less than 5%. Fig. 3b demonstrates changes in polarization 1 and polarization 2 during aging cycles. These polarizations respectively represent the change in polarization at the end of each discharging or charging cycle and can be defined using equations (1) and (2).

$$\text{Polarization 1} = V_{dis,end} - V_{rest\_dis,end}, \quad (1)$$

$$\text{Polarization 2} = V_{chg,end} - V_{rest\_chg,end}, \quad (2)$$

where $V_{dis,end}$ and $V_{chg,end}$ are voltages at the end of discharging and charging, respectively; $V_{rest\_dis,end}$ and $V_{rest\_chg,end}$ are voltage at the end of the rest right after discharging and charging, respectively. Since the voltage at the end of charging and discharging are held constant, polarization values provide quasi-thermodynamic information on the state of the positive electrode after each half cycle. Less negative values for polarization 1 indicate that the positive electrode material is more fully lithiated during the prior discharge, while less positive values for polarization 2 align with the extraction of more lithium from the NMC during charging. Polarization 2 is significantly less than polarization 1 in part due to kinetic aspects associated with the C/10 charge and a C/3 discharge.

While negligible differences between 6.9 kPa and 69 kPa are seen with respect to capacity, the polarization data shows two primary trends. For polarization 1, following the C/3 discharge, the lower pressure leads to a more negative value by about 10 mV. This result is expected as the higher pressure leads to reduced contact resistance at the interface between the electrodes and current collector, between positive electrode particles, and to variation in the lithium electrode morphology including enhanced contact between roughened/isolated parts of the electrode, all of which impact cell polarization [12]. At lower discharging rates during the RPTs, there is less difference in the polarization between the two pressure conditions. During normal cycling the overall trend for polarization 1 and 2 are counter to each other with polarization 1 becoming less negative while polarization 2 increases for both 6.9 and 69 kPa. Polarization 2 also has less discrete difference between the two pressure regimes. The lack of variance between pressures is likely due to the reduced rate (C/10) used for charging the cell which leads to a reduced impact of cell kinetic aspects. With respect to the difference in polarization 1 (~10 mV decrease) and polarization 2 (~2 mV increase), the variance can best be explained in the following way. As pressure increases and lower contact resistance across the cell is seen there is a more discrete change in polarization at higher rates such as the C/3 discharge which leads to an observed reduction in polarization. At lower rates such as the C/10 charge and during the RPTs the change is less pronounced and impedance increases as expected. Over cycling, contact resistance has an overall larger impact when the cell is in the discharged state as this is when the electrode is more likely to have a roughened surface with greater quantities of isolated lithium.

In Fig. 3c, a representative illustration of the voltage and pressure responses during a single cycle (i.e., cycle 10) for a cell, which had an initial pressure of 69 kPa, is shown. The pressure response has many similarities to the voltage profile where a plateau region is observed at lower voltages with greater change in pressure at higher voltage. For comparison, during cycle 1 (Supplemental Fig. 1), the change in pressure is more linear over the full duration of charging and discharging. This data mirrors previous reports that shows plateaus in pressure evolution for NMC-based LMBs [29].

Fig. 3d demonstrates normalized pressure changes for both 6.9 and 69 kPa during 25 aging cycles and the two RPTs. Normalized pressure changes are calculated based on $P_{current}/P_{initial}$, where $P_{initial}$ is either 6.9 or 69 kPa. The extent of normalized change varies with both the initial pressure and number of cycles. For both pressures, the pressure evolution can be loosely broken into three regions. In the first region (Region 1, first RPT), the change during charging and discharging is nearly uniform and there is not much change in peak pressure with each cycle. The second region (Region 2) sees a distinct increase in peak and valley pressure and the pressure reduction during discharging is less than the pressure increase during charging. In the third region (Region 3), the pressure is flatter again and changes during charging and discharging are more uniform. In the third region, which constitutes both normal and second RPT cycles, the pressure evolution per cycle is less than that observed in the Region 1. During the early stages of cycling, the general trend in pressure suggests that the bulk mechanical response of the cell, as indicated by pressure change, is mainly affected by processes at the negative electrode rather than the positive electrode, where NMC volume expansion/contraction occurs opposite to what is observed in Fig. 3c [28].

From Fig. 4a, it is clear that the voltage response of the cells does not change between RPT 1 and RPT 2. However, when looking at the change in pressure with respect to voltage between the two RPTs (Fig. 4b), it is clear that while the electrochemical response of the cell is nearly the same as the cell ages, change in the mechanical response is relatively significant. There is also a dramatic shift when moving from RPT 1 to RPT 2. At slow rates, dQ dV^{-1} analysis has been often used to assess the thermodynamic-based response from cells in a quasi-equilibrium state [33]. The data in Fig. 4c provides the differential analysis that corresponds with Fig. 4a. As expected, there is negligible variation both with respect to initial applied pressure and early life aging. This lack of variation shows that there is no distinguishable difference in electrochemical response at slow rates. In a similar vein, for the current study, differential pressure analysis (dP dV^{-1}) has been used to better understand the link between the mechanical and electrochemical response of LMBs. Note that the values of dQ dV^{-1} during charging and discharging are positive and negative, respectively. On the other hand, the values of dP dV^{-1} during charging and discharging are both positive. For comparison purposes, a positive dP dV^{-1} during discharging is intentionally converted to negative. In Fig. 4c, the intensity and position of the primary peak associated with Ni oxidation and reduction during both charging and discharging in the dQ dV^{-1} at 3.71 V hardly changes irrespective of pressure condition, which suggests that there is no distinct change in the electrochemical response of the positive electrode. Likewise, there is not a distinct shift in the alignment of the other electrochemical processes, as informed by the dQ dV^{-1}, either regarding intensity or position between the first and the second RPTs. In Fig. 4d, during RPT 1 the pressure response closely follows the electrochemical response where the largest change in pressure aligns with the Ni redox behavior and a steady pressure increase aligns with the solid-solution electrochemistry at higher voltages. While the general shape of the curve is the same during RPT 2, the intensity of the pressure change near 3.71 V is dramatically reduced at both pressures, whereas there is minimal difference at high voltage.

To further investigate battery degradation mechanisms, dP dV^{-1} curves during charging and discharging are plotted at cycle 2, 15, and 23 from the cycle aging set in Fig. 5. Whereas the data in Fig. 4 is from the RPTs where charging and discharging were both at a C/20 rate, the charging and discharging data in Fig. 5 is at C/10 (charge) and C/3 (discharge) rate, respectively. Broadly, the trends observed in Fig. 5 mirror those observed in Fig. 4a, and no distinct changes of the primary dQ dV^{-1} peaks are visible. For the dP dV^{-1}, both the primary peak near 3.71 V and the higher voltage plateau exhibit significant intensity reduction from cycle 2 to cycle 15. Between cycles 15 and 23, only minor changes in the dP dV^{-1} response are observed. The reduction at 3.71 V is consistent with the slower rate in Fig. 4, but the reduced dP dV^{-1} at higher voltages is more pronounced at the higher discharging rate.

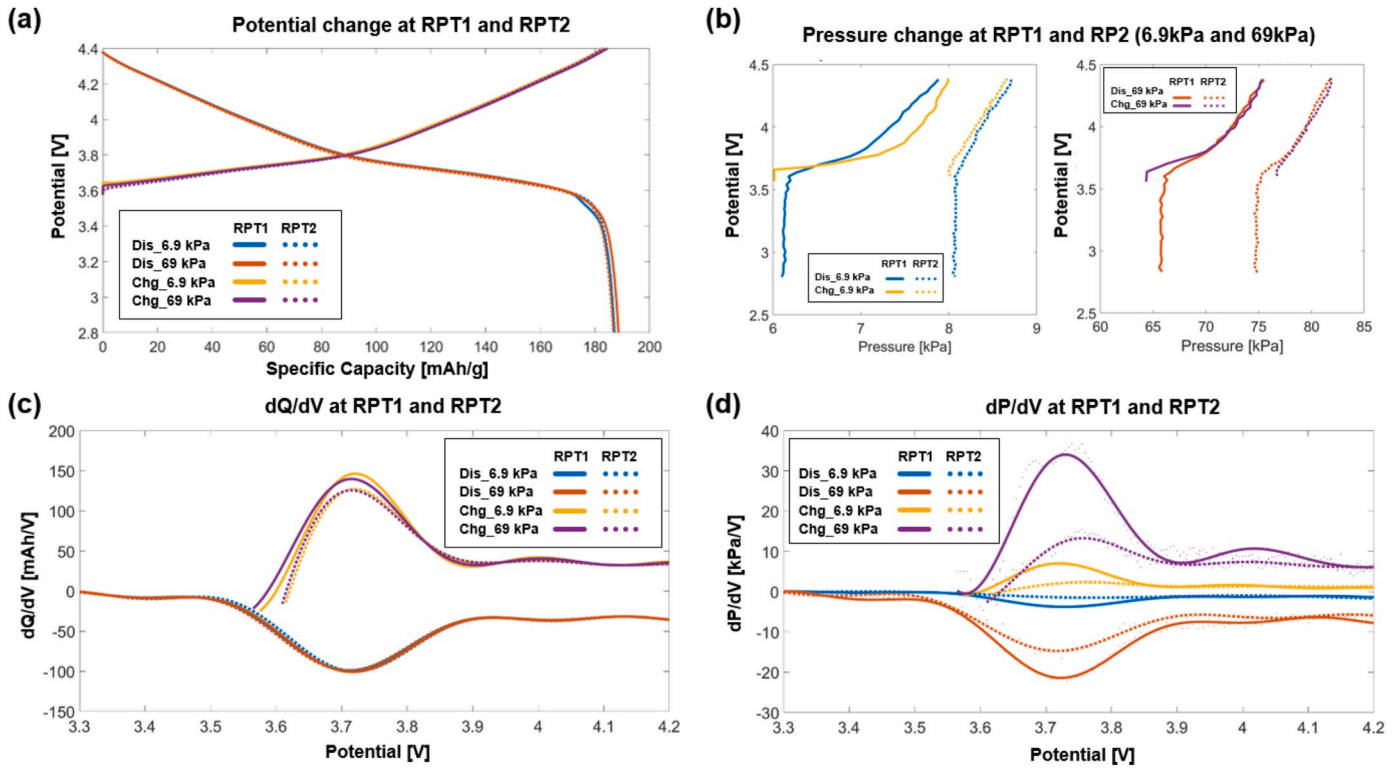

Fig. 4. (a) Potential change, (b) pressure change, (c) dQ dV^{-1}, and (d) dP dV^{-1} at the first RPT and the second RPT under 6.9 kPa and 69 kPa.

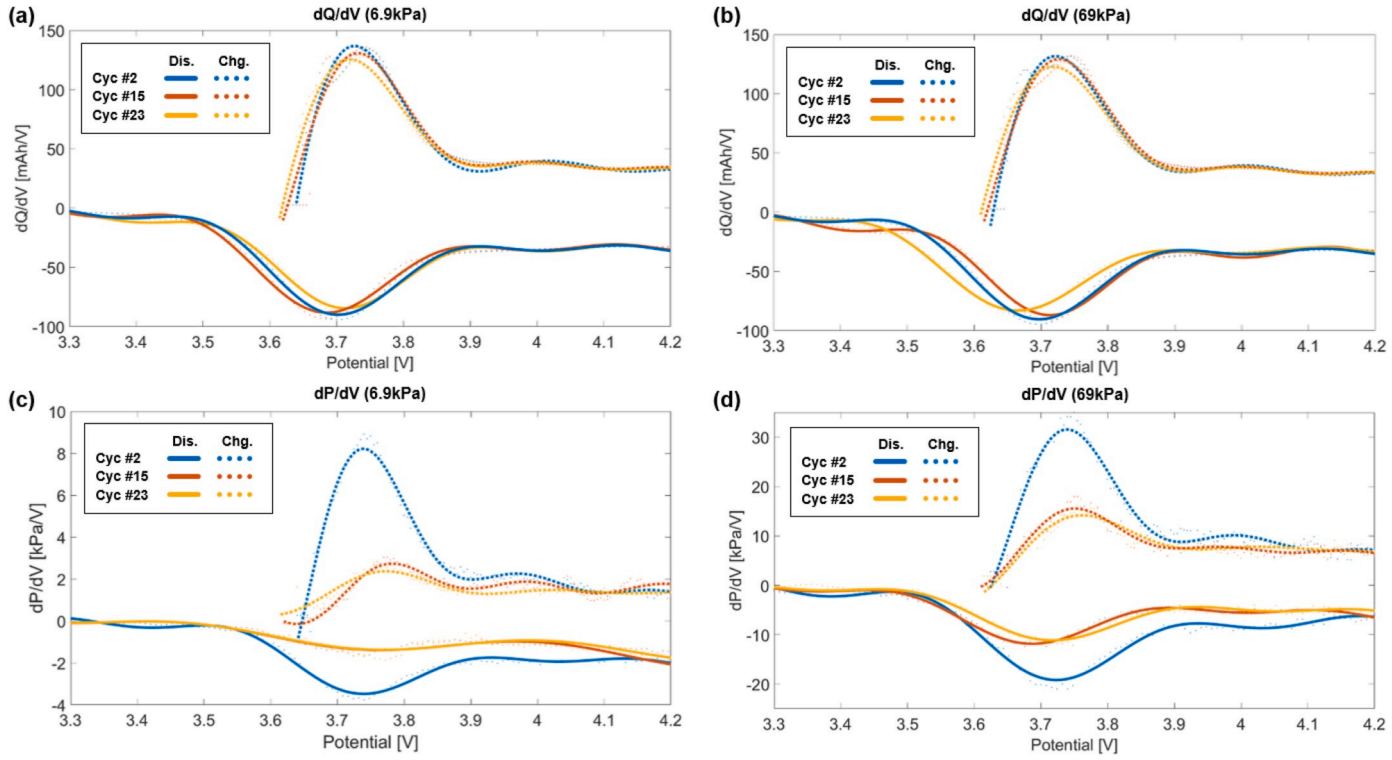

Fig. 5. dQ dV^{-1} under (a) 6.9 kPa and (b) 69 kPa and dP dV^{-1} under (a) 6.9 kPa and (b) 69 kPa at the cycle 2, 15, and 23.

4. Discussion

As detailed above, there are both similarities and clear differences between the electrochemical (dQ dV^{-1}) and mechanical (dP dV^{-1}) performance of LMBs. Three different mechanical responses of the cell, which is shown in the pressure data, are the peak pressure (pressure at the end of charging), valley pressure (pressure at the end of discharging), and the pressure change during a given cycle. In tracking these mechanical responses on a cycle-by-cycle basis, three regions can be clearly defined with respect to the alignment of electrochemical and

mechanical responses.

In the first region, which is depicted in Fig. 6a and d and Fig. S2a, the alignment suggests that the early deposition and stripping processes occur in a uniform manner and the bulk of the plated lithium remains electrochemically active. The surface starts as a smooth lithium film enabling plating and stripping to occur in a uniform manner resulting in minor losses and little net increase in cycle-to-cycle pressure. In the first region, there is close alignment of the electrochemical (dQ dV^{-1}) and mechanical (dP dV^{-1}) responses.

The second region, which occurs during the first few cycles after RPT 1 (Fig. 6b and e and Fig. S2b), is defined by increased peak and valley pressures, little change in capacity and relatively uniform increase in pressure during each charging process. While the overall pressure increases in a cycle-by-cycle manner, there is little observed capacity decay and no distinct change in dQ dV^{-1} response at either pressure (Fig. 5a and b). The distinct build-up of pressure in this region over cycling for both peak and valley pressures suggests that the overall electrode thickness is increasing in an irreversible manner through processes such as change in the surface due to dendritic, porous lithium morphology evolution, and the formation of dead lithium and SEI [34]. However, despite the increase in electrode thickness, the low levels of capacity loss of less than 5% capacity fade between the RPTs is a strong indicator that excess lithium in the negative electrode is still accessible. The growth of thick lithium electrodes with high porosity is well known in the literature, but few reports of *in operando* measurements which can link back to the mechanical and structural evolution exist.

While an increase in peak/valley pressure is observed during the early cycles, it is followed by a relatively consistent peak pressure and valley pressure. This third region in Fig. 6c and f and Fig. S2c is indicative of a more steady-state mechanical condition in the cell where the overall thickness of the negative electrode maintains a more constant thickness than that observed near the beginning of life for the LMB. Overall, the pressure changes are unique in that the change in pressure is changing by only about 1/2 of what occurs during early cycling, while the cycled capacity is close to 95% that of the beginning of life. This phenomenon is uniform for both pressures investigated here though it occurs slightly earlier in cycling at 6.9 kPa (Fig. 3d). The attainment of a steadier increase after some level of cycling can be explained in the following way: 1) as cycling progresses the structure of the negative electrode becomes more porous. The evolution of dense lithium towards higher porosity has been previously shown using simulation and post-test cell characterization [28,35]. 2) After extensive cycling the lithium electrode is dictated by regions of porous electrode with increased presence of lithium which is either electrochemically isolated or which is part of the SEI. In this region smaller pressure change occurs as an increasing amount of lithium is plated and stripped from the interior of the now porous negative electrode. In the third region, rather than the case at the beginning of life (Region 1) where the active lithium front is adjacent to the separator, the reactive lithium is now buried in the electrode and the inactive 'dead' lithium is adjacent to the separator. As such, as the cell ages, inactive lithium becomes the predominant observed species in post-test electrode imaging [36]. 3) Lastly, little increase in cycle-to-cycle pressure is seen in Region 3 since most of the new 'dead' lithium is also in the pores and interior of the electrode, which was confirmed by SEM and ion beam images in Fig. 6f and Fig. S2c.

While the presence of different regions described above hold for both pressure conditions investigated here, there are two other distinct insights from this study which pertain to the evolution of the electrochemical and mechanical status of the LMBs. From Figs. 4 and 5, it is evident that the peak intensity in the dP dV^{-1} plots are more sensitive to evolution in the electrode structure than traditional analysis methods including dQ dV^{-1} as cycling progresses. Using the normalized intensity for these peaks (starting at cycle 1 following the RPT) allows a clearer identification of when different regions in the structural evolution of the electrode occur (Fig. 7). Since the current study focused on demonstrating the alignment of electrochemical and mechanical data using an electrolyte, which is not ideal for lithium plating and stripping, the first region is not clearly shown in Fig. 7 as it largely occurs during the slower cycling RPT. Instead, both conditions show a transition over the first three cycles before reaching a plateau at just below 0.65. This plateau is associated with Region 2 in Fig. 6 above. For the remainder of the first 15 cycles the higher pressure 69 kPa condition has no other distinct changes in the normalized peak intensity suggesting that it remains in this region for the duration of these cycles. On the other hand, the lower pressure 6.9 kPa cells undergoes a second reduction in intensity between

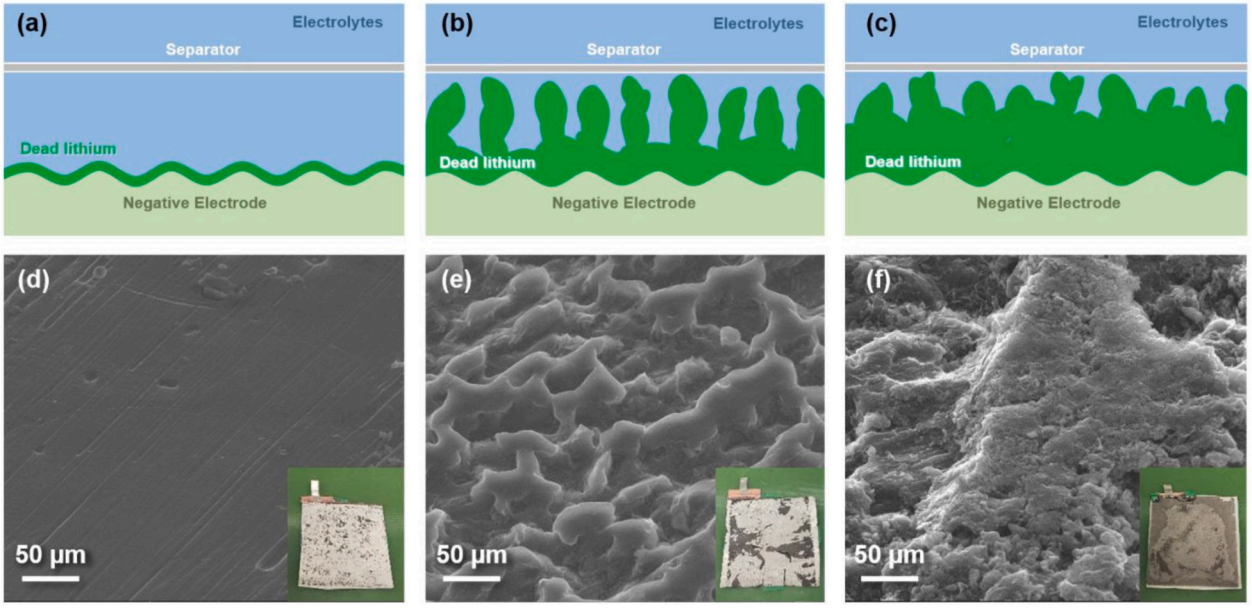

Fig. 6. (a–c) Schematic illustration and (d–f) SEM images of the lithium electrode at different stages of cycling The inset shows the lithium metal electrode from cycled pouch cells after full discharge. Three regions are defined during dead lithium development; (a, d) Region 1: Initial surface of the negative electrode, (b, e) Region 2: porous electrode surface developed, and (c,f) Region 3: Build-up of dead lithium and a more complex surface layer with fewer deep ridges present. Insets show the full electrode image indicating that significant variation occurs across the lithium electrode surface.

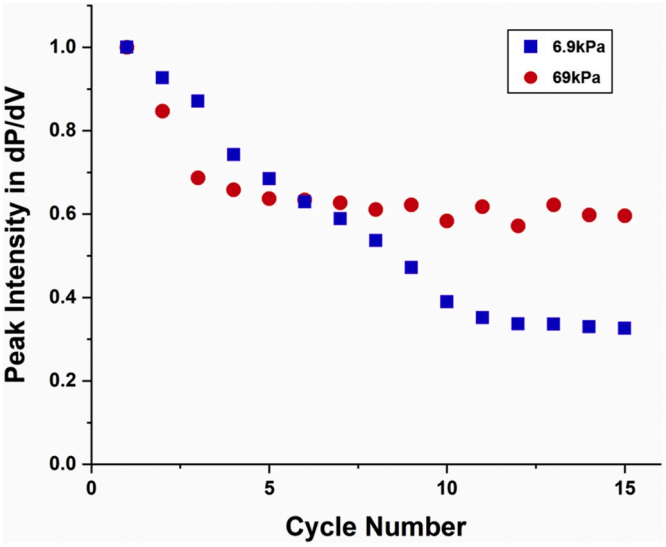

Fig. 7. Normalized peak intensity for the charging peak at 3.71 V through the first 15 cycles.

cycles 6 and 10 before reaching a second plateau at around a normalized intensity of ~0.3. This aligns with Region 3 in Fig. 6. The extended period of time that the higher pressure cell remains in Region 2 aligns well with previous reports that increased pressure benefits extended the life of LMBs [22,30]. By applying the higher pressure and tracking the evolution of the dP dV^{-1} signal, it is possible to track that using the higher pressure 69 kPa maintained a denser electrode structure longer and maintained the active lithium front closer to the separator.

The second key distinct insight is more closely associated with the nature of how and when a cycle pressure evolution occurs within the cell. In Figs. 4 and 5, there is little dP dV^{-1} change as a function of cycling at voltages greater than 3.9 V in either the charging or discharging directions. Counter to that, there is a very distinct change near 3.71 V where the pressure evolution is significantly reduced as the cells cycle. Based on how these peaks align with electrode processes, the dP dV^{-1} data suggests that a significant portion of the lithium plated during the charging is in the porous layers of the cell leading to less increase in electrode thickness and hence pressure increase as a porous negative electrode evolves during cycling. Near the end of charging, regardless of the extent of electrode porosity, most of the plated lithium is near the exterior of the electrode creating a more reproducible pressure signature. During discharging, the inverse occurs where lithium is first stripped from the exterior of the electrode and then form more porous electrode regions. Possibly exacerbating the reduced pressure near 3.71 V is that this is the region where most of the volume change associated with NMC lithiation and delithiation occurs [14]. NMC expands during lithiation (discharging) and contracts during delithiation (charging) by about 10%, thus pressure changes from NMC are counter to that seen due to lithium metal plating and stripping. While the NMC likely plays a role in the mechanical response, the lack of change in pressure response with cycling at higher voltage supports the bulk of the mechanical response being associated with enhanced negative electrode porosity as cycling advances. Previous work has distinctly shown that as LMBs age, they tend to have increasingly worse rate performance [8,36]. Taking the information from this work, this aging phenomenon can be better explained as lithium-ions need to travel a more tortuous path during charging and discharging as the lithium electrode transitions from Region 1 to 3 in Fig. 7.

5. Conclusions

The complimentary analysis of electrochemical and mechanical data presents the possibility to more clearly understand the aging phenomena of LMBs. Here, differential pressure (dP dV^{-1}) analysis is used to align how the mechanical evolution of the lithium metal negative electrode compares to electrochemical cycling data. During cycling, it was found that the mechanical data provides distinct information on cycling that is not easily discernible from the electrochemical capacity of the cell. Using dP dV^{-1}, the evolution of the lithium metal electrode can be tracked *in operando* as the electrode transitions from a planar system to a more tortuous, and porous electrode structure. The pressure data also elucidate the nature of lithium plating on the negative electrode. As the cells age, the initial lithium is plated in the interior of the electrode generating a diminished dP dV^{-1} response. Later in the cycle, lithium is plated on the exterior of the electrode. During discharging, the inverse trend is observed. As a set of complimentary methods, the combination of pressure and electrochemical response provide an opportunity to more directly follow the state of LMBs and may help in the early identification of cell failure. While the present work focused on a NMC622 positive electrode, the findings on the impacts at the negative electrode should hold for other positive electrodes. That said, as the volume expansion of different positive materials varies, it is expected that some nuance in the mechanical response should be evident as the materials are integrated into LMBs. Future works extending this study are planned along these lines to include the application of a dP dV^{-1} analysis for other battery chemistries including other positive electrode materials and electrolytes. Additionally higher initial stack pressures will be investigated to further elucidate the role that pressure plays in improving performance.

Declaration of competing interest

The authors declare that they have no known competing financial interests or personal relationships that could have appeared to influence the work reported in this paper.

CRediT authorship contribution statement

Sangwook Kim: Writing - original draft, Writing - review & editing, Data curation. **Abhi Raj:** Writing - review & editing. **Bin Li:** Writing - original draft, Data curation, Writing - review & editing. **Eric J. Dufek:** Writing - original draft, Writing - review & editing, Data curation. **Charles C. Dickerson:** Writing - original draft, Writing - review & editing. **Hsiao-Ying Huang:** Supervision, Data curation, Writing - review & editing. **Boryann Liaw:** Writing - review & editing, Data curation. **Gorakh M. Pawar:** Writing - review & editing, Data curation.

Acknowledgements

Research has been supported by the Assistant Secretary for Energy Efficiency and Renewable Energy, Office of Vehicle Technologies of the U.S. Department of Energy through the Advanced Battery Materials Research Program (Battery 500 Consortium). INL is operated by Battelle Energy Alliance under Contract Nos. DE-AC07-05ID14517 for the U.S. Department of Energy. The authors would like to thank Andrew Jansen and Bryant Polzin at the Cell Analysis Modeling and Prototyping (CAMP) facility at Argonne National Laboratory for providing positive electrode laminates used in this study. The U.S. Government retains and the publisher, by accepting the article for publication, acknowledges that the United States Government retains a nonexclusive, paid-up, irrevocable, world-wide license to publish or reproduce the published form of this manuscript, or allow others to do so, for U.S. Government purposes.

Appendix A. Supplementary data

Supplementary data to this article can be found online at https://doi.org/10.1016/j.jpowsour.2020.228180.

References

[1] J. Liu, Z. Bao, Y. Cui, E.J. Dufek, J.B. Goodenough, P. Khalifah, Q. Li, B.Y. Liaw, P. Liu, A. Manthiram, Y.S. Meng, V.R. Subramanian, M.F. Toney, V. V. Viswanathan, M.S. Whittingham, J. Xiao, W. Xu, J. Yang, X.Q. Yang, J.G. Zhang, Pathways for practical high-energy long-cycling lithium metal batteries, Nat. Energy. 4 (2019) 180–186, https://doi.org/10.1038/s41560-019-0338-x.

[2] J. Zheng, M.H. Engelhard, D. Mei, S. Jiao, B.J. Polzin, J.G. Zhang, W. Xu, Electrolyte additive enabled fast charging and stable cycling lithium metal batteries, Nat. Energy. 2 (2017), https://doi.org/10.1038/nenergy.2017.12.

[3] F. Xin, H. Zhou, X. Chen, M. Zuba, N. Chernova, G. Zhou, M.S. Whittingham, -O. Li-Nb, Coating/substitution enhances the electrochemical performance of the LiNi0.8Mn0.1Co0.1O2 (NMC 811) cathode, ACS Appl. Mater. Interfaces 11 (2019) 34889–34894, https://doi.org/10.1021/acsami.9b09696.

[4] H. Zhou, F. Xin, B. Pei, M.S. Whittingham, What limits the capacity of layered oxide cathodes in lithium batteries? ACS Energy. Lett. 4 (2019) 1902–1906, https://doi.org/10.1021/acsenergylett.9b01236.

[5] G. Liu, W. Lu, A model of concurrent lithium dendrite growth, SEI growth, SEI penetration and regrowth, J. Electrochem. Soc. 164 (2017) A1826–A1833, https://doi.org/10.1149/2.0381709jes.

[6] K.H. Chen, A.J. Sanchez, E. Kazyak, A.L. Davis, N.P. Dasgupta, Synergistic effect of 3D current collectors and ALD surface modification for high coulombic efficiency lithium metal anodes, Adv. Energy Mater. 9 (2019) 1–12, https://doi.org/10.1002/aenm.201802534.

[7] K.N. Wood, M. Noked, N.P. Dasgupta, Lithium metal anodes: toward an improved understanding of coupled morphological, electrochemical, and mechanical behavior, ACS Energy. Lett. 2 (2017) 664–672, https://doi.org/10.1021/acsenergylett.6b00650.

[8] S.C. Nagpure, T.R. Tanim, E.J. Dufek, V.V. Viswanathan, A.J. Crawford, S. M. Wood, J. Xiao, C.C. Dickerson, B. Liaw, Impacts of lean electrolyte on cycle life for rechargeable Li metal batteries, J. Power Sources 407 (2018) 53–62, https://doi.org/10.1016/j.jpowsour.2018.10.060.

[9] S. Kim, H.Y.S. Huang, Mechanical stresses at the cathode-electrolyte interface in lithium-ion batteries, J. Mater. Res. 31 (2016) 3506–3512, https://doi.org/10.1557/jmr.2016.373.

[10] S. Kim, J. Wee, K. Peters, H.Y.S. Huang, Multiphysics coupling in lithium-ion batteries with reconstructed porous microstructures, J. Phys. Chem. C. 122 (2018) 5280–5290, https://doi.org/10.1021/acs.jpcc.7b12388.

[11] R. Xu, H. Sun, L.S. de Vasconcelos, K. Zhao, Mechanical and structural degradation of LiNixMnyCozO2 cathode in Li-ion batteries: an experimental study, J. Electrochem. Soc. 164 (2017) A3333–A3341, https://doi.org/10.1149/2.1751713jes.

[12] Y.C. Zhang, O. Briat, J.Y. Deletage, C. Martin, G. Gager, J.M. Vinassa, Characterization of external pressure effects on lithium-ion pouch cell, Proc. IEEE Int. Conf. Ind. Technol. (2018) 2055–2059, https://doi.org/10.1109/ICIT.2018.8352505, 2018-Febru.

[13] C.K. ChiuHuang, H.Y. Shadow Huangz, Stress evolution on the phase boundary in LiFePO4 particles, J. Electrochem. Soc. 160 (2013) 2184–2188, https://doi.org/10.1149/2.079311jes.

[14] R. Koerver, W. Zhang, L. De Biasi, S. Schweidler, A.O. Kondrakov, S. Kolling, T. Brezesinski, P. Hartmann, W.G. Zeier, J. Janek, Chemo-mechanical expansion of lithium electrode materials-on the route to mechanically optimized all-solid-state batteries, Energy Environ. Sci. 11 (2018) 2142–2158, https://doi.org/10.1039/c8ee00907d.

[15] R. Jung, M. Metzger, F. Maglia, C. Stinner, H.A. Gasteiger, Oxygen release and its effect on the cycling stability of LiNixMnyCozO2 (NMC) cathode materials for Li-ion batteries, J. Electrochem. Soc. 164 (2017) A1361–A1377, https://doi.org/10.1149/2.0021707jes.

[16] W.J. Zhang, A review of the electrochemical performance of alloy anodes for lithium-ion batteries, J. Power Sources 196 (2011) 13–24, https://doi.org/10.1016/j.jpowsour.2010.07.020.

[17] C. Fang, X. Wang, Y.S. Meng, Key issues hindering a practical lithium-metal anode, Trends Chem. 1 (2019) 152–158, https://doi.org/10.1016/j.trechm.2019.02.015.

[18] A.J. Louli, L.D. Ellis, J.R. Dahn, Operando pressure measurements reveal solid electrolyte interphase growth to rank Li-ion cell performance, Joule 3 (2019) 745–761, https://doi.org/10.1016/j.joule.2018.12.009.

[19] A.J. Louli, J. Li, S. Trussler, C.R. Fell, J.R. Dahn, Volume, pressure and thickness evolution of Li-ion pouch cells with silicon-composite negative electrodes, J. Electrochem. Soc. 164 (2017) A2689–A2696, https://doi.org/10.1149/2.1691712jes.

[20] J. Li, L.E. Downie, L. Ma, W. Qiu, J.R. Dahn, Study of the failure mechanisms of LiNi0.8Mn0.1Co0.1O2 cathode material for lithium ion batteries, J. Electrochem. Soc. 162 (2015) A1401–A1408, https://doi.org/10.1149/2.1011507jes.

[21] D. Nicholas, Williard, Effects of External Pressure on Solid State Diffusion of Lithium in Lithium-Ion Batteries, University of Maryland, 2016. http://hdl.handle.net/1903/19052.

[22] R. Weber, M. Genovese, A.J. Louli, S. Hames, C. Martin, I.G. Hill, J.R. Dahn, Long cycle life and dendrite-free lithium morphology in anode-free lithium pouch cells enabled by a dual-salt liquid electrolyte, Nat. Energy. 4 (2019) 683–689, https://doi.org/10.1038/s41560-019-0428-9.

[23] S. Torai, M. Nakagomi, S. Yoshitake, S. Yamaguchi, N. Oyama, State-of-health estimation of LiFePO 4/graphite batteries based on a model using differential capacity, J. Power Sources 306 (2016) 62–69, https://doi.org/10.1016/j.jpowsour.2015.11.070.

[24] M. Dubarry, M. Berecibar, A. Devie, D. Anseán, N. Omar, I. Villarreal, State of health battery estimator enabling degradation diagnosis: model and algorithm description, J. Power Sources 360 (2017) 59–69, https://doi.org/10.1016/j.jpowsour.2017.05.121.

[25] T.R. Tanim, M.G. Shirk, R.L. Bewley, E.J. Dufek, B.Y. Liaw, Fast charge implications: pack and cell analysis and comparison, J. Power Sources 381 (2018) 56–65, https://doi.org/10.1016/j.jpowsour.2018.01.091.

[26] T. Shibagaki, Y. Merla, G.J. Offer, Tracking degradation in lithium iron phosphate batteries using differential thermal voltammetry, J. Power Sources 374 (2018) 188–195, https://doi.org/10.1016/j.jpowsour.2017.11.011.

[27] M. Berecibar, M. Dubarry, N. Omar, I. Villarreal, J. Van Mierlo, Degradation mechanism detection for NMC batteries based on Incremental Capacity curves, World Electr. Veh. J. 8 (2016) 350–361.

[28] C. Niu, H. Lee, S. Chen, Q. Li, J. Du, W. Xu, J.G. Zhang, M.S. Whittingham, J. Xiao, J. Liu, High-energy lithium metal pouch cells with limited anode swelling and long stable cycles, Nat. Energy. 4 (2019), https://doi.org/10.1038/s41560-019-0390-6.

[29] A. Raj, C.C. Dickerson, S.C. Nagpure, S. Kim, C. Niu, J. Xiao, B. Liaw, E.J. Dufek, Communication - pressure evolution in constrained rechargeable lithium-metal pouch cells, J. Electrochem. Soc. 167 (2020), 020511, https://doi.org/10.1149/1945-7111/abd6439.

[30] Y. Zhang, F.M. Heim, N. Song, J.L. Bartlett, X. Li, New insights into mossy Li induced anode degradation and its formation mechanism in Li-S batteries, ACS Energy. Lett. 2 (2017) 2696–2705, https://doi.org/10.1021/acsenergylett.7b00886.

[31] H. Kim, Y.J. Gong, J. Yoo, Y.S. Kim, Highly stable lithium metal battery with an applied three-dimensional mesh structure interlayer, J. Mater. Chem. A. 6 (2018) 15540–15545, https://doi.org/10.1039/c8ta05069d.

[32] H. Lee, J. Song, Y.J. Kim, J.K. Park, H.T. Kim, Structural modulation of lithium metal-electrolyte interface with three-dimensional metallic interlayer for high-performance lithium metal batteries, Sci. Rep. 6 (2016) 1–10, https://doi.org/10.1038/srep30830.

[33] M. Dubarry, B.Y. Liaw, Identify capacity fading mechanism in a commercial LiFePO4 cell, J. Power Sources 194 (2009) 541–549, https://doi.org/10.1016/j.jpowsour.2009.05.036.

[34] A.J. Louli, M. Genovese, R. Weber, S.G. Hames, E.R. Logan, J.R. Dahn, Exploring the impact of mechanical pressure on the performance of anode-free lithium metal cells, J. Electrochem. Soc. 166 (2019) A1291–A1299, https://doi.org/10.1149/2.0091908jes.

[35] A. Aryanfar, D.J. Brooks, A.J. Colussi, B.V. Merinov, W.A. Goddard, M. R. Hoffmann, Thermal relaxation of lithium dendrites, Phys. Chem. Chem. Phys. 17 (2015) 8000–8005, https://doi.org/10.1039/c4cp05786d.

[36] Y. Zhang, Q. Wang, B. Liaw, S.C. Nagpure, E.J. Dufek, C.C. Dickerson, A quantitative failure analysis on capacity fade in rechargeable lithium metal cells lithium metal cells, J. Electrochem. Soc. 167 (2020), https://doi.org/10.1149/1945-7111/ab6cf4.

Supplementary Information

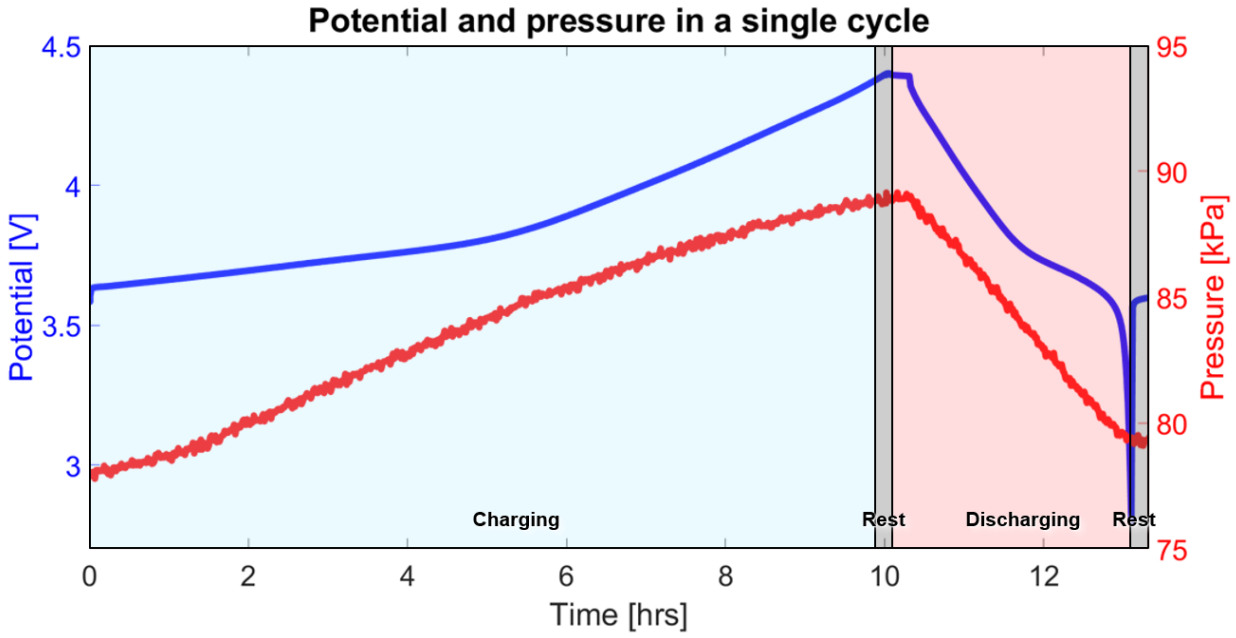

Figure S1. Potential and pressure changes in cycle 1 for a cell, which had an initial pressure of 69 kPa.

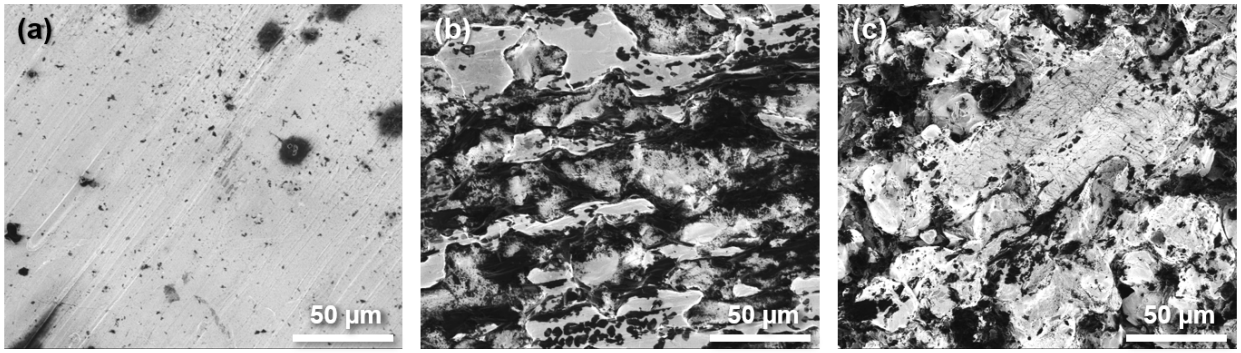

Figure S2. Ion beam images of (a)Region1, (b) Region 2, and (c) Region 3